Applied Catalysis B: Environmental 162 (2015) 475–482

Contents lists available at ScienceDirect

Applied Catalysis B: Environmental

journal homepage: www.elsevier.com/locate/apcatb

Gold nanoparticles supported on modified red mud for biphasic oxidation of sulfur compounds: A synergistic effect

Aline A.S. Oliveira, Demétrio A.S. Costa, Ivo F. Teixeira, Flávia C.C. Moura*

Departamento de Química, ICEx, Universidade Federal de Minas Gerais, Av. Antônio Carlos, 6627, Pampulha, Belo Horizonte, MG, CEP 31270-901, Brazil

ARTICLE INFO

Article history:
Received 10 April 2014
Received in revised form 5 June 2014
Accepted 1 July 2014
Available online 17 July 2014

Keywords:
Red mud
Gold
Desulfurization
Synergistic effect

ABSTRACT

Gold nanoparticles were supported on the surface of three different matrixes based on red mud waste: (i) pure red mud, (ii) reduced red mud and (iii) partially carbon coated red mud, in order to produce different catalysts for desulfurization reactions. The catalysts were extensively characterized by X-ray diffraction, Mössbauer spectroscopy, thermogravimetric analyses, electron microscopies (SEM and TEM), energy dispersive spectroscopy (EDS) and BET surface area. Results showed that gold was successfully supported and distributed on the surface of red mud based materials as nanoparticles with diameters around 30 nm. The catalyst prepared with carbon coated red mud has shown to be twice more efficient than others for biphasic desulfurization reactions. This result can be associated with its amphiphilicity, which allows the catalyst to be located on the interface of biphasic systems. In this position a synergistic effect occurs between gold nanoparticles that adsorb S containing molecules and red mud Fe sites that promote the formation of OH radicals. The same effect is not observed for catalyst with hydrophilic supports.

© 2014 Elsevier B.V. All rights reserved.

1. Introduction

Red mud (Rm) is the waste by-product of the Bayer process used to extract alumina (Al_2O_3) from bauxite ores for the production of aluminum metal [1]. It is estimated that for each ton of alumina (Al_2O_3) produced, 0.5–2 ton (on a dry weight basis) of red mud are generated with a global production of about 120 million tons of red mud per year [1,2]. Rm poses several environmental hazards due to its high alkalinity (pH >11), sodium and heavy metal contents [2] and, in some cases, some large volumes are stored in inappropriate areas. In 2010, a red mud reservoir in Hungary collapsed and an amount around 700,000 m^3 of mud with a pH around 12 was released from the reservoir to the nearby cities [3].

In this context, the development of technologies to give red mud a proper destination is of great interest. Rm has been applied in different areas [4], especially in catalysis. Its properties such as iron content mainly as ferric oxide (Fe_2O_3), relatively high surface area, sintering resistance, resistance to poisoning and low cost make it an attractive potential catalyst for many reactions [5]. Rm has been applied recently to several kinds of catalytic reactions: hydrodechlorinations [6], hydrogenations [7–9], coal liquefaction [10], biomass liquefaction [11], bio-oil upgrade [12,13], catalytic pyrolysis [14], conversion of waste oil and plastic [15], methane combustion [16], ammonia decomposition [17], methane conversion into syngas [18], hydrocracking reductions [19], biodiesel production [20], biphasic reactions [21,22] and oxidations [21,23,24]. One of the oxidation reactions widely studied recently is the oxidation of sulfur compounds in petroleum [25–28], also known as oxidesulfurization (ODS). It is well know that the sulfur impurities present in fuels are an important source of air pollution, acid rain and they also affect pollution control devices. In order to decrease pollution, ever-stricter legislation has been implemented all over the world to limit the content of sulfur in petroleum fuels. And for this reason, the development of new technologies for sulfur removal is necessary [29].

The deep oxidesulfurization depends on high selectivity of the catalyst due to low sulfur concentrations (less than 50 ppm). In order to improve the Rm capability to remove sulfur contaminants, this work investigated the activity of gold catalysts prepared with different Rm supports. Gold nanoparticles have a differentiated affinity for sulfur [30–32] and were used to enhance the activity of Rm supports in the oxidation of sulfur compounds. The catalysts prepared by gold nanoparticles and active supports may have different and exclusive properties due to a synergistic effect between them.

* Corresponding author. Tel.: +55 31 3409 7556; fax: +55 31 3409 5700.
E-mail address: flaviamoura@ufmg.br (F.C.C. Moura).

http://dx.doi.org/10.1016/j.apcatb.2014.07.003
0926-3373/© 2014 Elsevier B.V. All rights reserved.

Hereon are described recent results involving the preparation and characterization of different red mud materials with supported gold nanoparticles and their application in the oxidation of sulfur contaminants of petroleum fuels.

2. Experimental

2.1. Synthesis of supports and catalysts

Three different supports based on Red Mud residue were produced, i.e. Rm, RmH_2 and RmEt. Raw red mud suspension was obtained from ALCAN. The first support, Rm, corresponds to the raw residue suspension washed with distillated water and dried at 80 °C. In order to produce the second support, RmH_2, the dried Rm was submitted to a reduction reaction with H_2 up to 700 °C for 3 h with heating rate of 10 °C min^{-1}. For the synthesis of RmEt support, a CVD (Chemical Vapor Deposition) reaction was carried out with dried Rm and ethanol as carbon source. The system was also heated up to 700 °C for 3 h with rate of 10 °C min^{-1} but under flow of ethanol.

The gold complex $Au(en)_2Cl_3$ was first synthesized. 100 mg of $HAuCl_4{\cdot}3H_2O$ was stirred with 1 mL of Milli-Q water until complete solubilization. Then 45 μL of ethylenediamine was inserted together with 7.0 mL of ethanol. After 20 min the complex could be purified by centrifugation followed by separation of the supernatant, washing the precipitate with ethanol and drying under vacuum.

The catalysts were produced with 54 mg of the complex $Au(en)_2Cl_3$ and 500 mg of the support (Rm, RmH_2 or RmEt) in order to obtain materials with 5% of Au. Around 150 mL of Milli-Q water was added to this mixture, leaving it stirring for about 15 min. The mixture was then heated up to 70 °C and kept under magnetic stirring until complete evaporation of water and it was finally dried under vacuum and in an oven at 65 °C for about 14 h. A red powder was obtained, which was heated (10 °C min^{-1}) up to 300 °C for 2 h under N_2 atmosphere (to prevent any oxidation or damage to the structure of Rm).

2.2. Synthesis and characterization of the catalysts

Supports and catalysts were characterized by different techniques, i.e. temperature programmed reduction (TPR), X-ray diffraction – XRD, Mössbauer spectroscopy, thermal analyses – TG/DTA, electron microscopies – SEM and TEM, EDS microanalysis, particles size distribution and surface area and porosity by the BET method.

TPR analyses were carried out using a CHEM BET 3000 TPR Quantachrome equipment equipped with a thermal conductivity detector (TCD) with H_2 (5% in N_2) and heating rate of 10 °C min^{-1}. The powder XRD data WAS obtained in a Rigaku model Geigerflex equipment using Co Kα radiation scanning from 10 to 80° (2θ) at a scan rate of 4° min^{-1}. Silicon was used as an external standard. The transmission Mössbauer spectroscopy experiments were carried out in a spectrometer CMTE model MA250 with a $^{57}Co/Rh$ source at room temperature using α-Fe as a reference. TG analyses were carried out in a Shimadzu TGA-60, with a constant heating rate of 10 °C min^{-1} under air flow (100 mL min^{-1}). The surface area was determined by nitrogen adsorption using the BET method with a 22 cycles N_2 adsorption/desorption in an Autosorb 1 Quantachrome instrument. Electron microscopies analyses were performed using a microscope SEG – Quanta 200 – SEI for SEM and a microscope Tecnai G2 200 kV – SEI for TEM. Analyses by energy dispersive spectroscopy (EDS) were performed in a JEOL JXA-8900 RL where samples were submitted to 15 kV voltage.

2.3. Catalytic reactions

The gold catalysts and also their pure supports were employed in heterogeneous Fenton reactions in biphasic systems for the oxidation of dibenzothiophene (DBT). Reactions were carried out with 5 mL of organic phase (50 mg L^{-1} S of DBT in cyclohexane), 1 mL of oxidant aqueous phase (H_2O_2 30%) and 20 mg of the catalyst. DBT removal was monitored by UV–vis spectroscopy (Shimadzu UV-2550 with photomultiplier detector R-928).

3. Results and discussion

Gold nanoparticles were impregnated on the surface of three different supports based on red mud (Rm) residue: (i) Pure Rm, (ii) Rm reduced with H_2, and finally (iii) Rm after CVD reaction with ethanol. Besides being hazardous and very available, red mud residue is rich in iron oxides (~30%), species of great chemical interest. It also contains thermally stable oxides, i.e. Al_2O_3 and SiO_2, which provide stability to the materials produced. The main disadvantages of pure Rm for the processes studied in this work are: (i) it is not magnetic, (ii) it may suffer leaching, (iii) it presents low surface area and (iv) it is very hydrophilic. In order to overcome these limitations, two supports based on Rm were prepared: (a) Rm reduced with H_2, a magnetic material that does not suffer leaching, and (b) Rm after CVD with ethanol, a magnetic material partially coated with carbon, which does not suffer leaching, has higher surface area and is amphiphilic. These supports led to the catalysts Au/Rm, Au/RmH_2 and Au/RmEt, respectively. These catalysts were extensive characterized in order to obtain information about their structure, morphology, iron phases, composition, surface area and porosity.

In order to characterize the crystalline phases formed in the catalysts Au/Rm, Au/RmH_2 and Au/RmEt, X-ray diffraction (XRD) was used. Fig. 1 shows X-ray diffraction patterns obtained for the three catalysts.

Some peaks related to metallic Au are observed in all XRD patterns of Fig. 1, showing that the impregnation method was efficient and Au was supported on the Rm materials in a crystalline form. The metallic Au phase was characterized according to PDF 1-1172.

In the sample Au/Rm, hematite is identified (PDF 1-1053) as the only crystalline iron phase. It is also possible to observe a characteristic peak of Al_2O_3 (2θ = 33°, PDF 10-414). As Rm has a complex composition, it is possible that peaks relating to other common

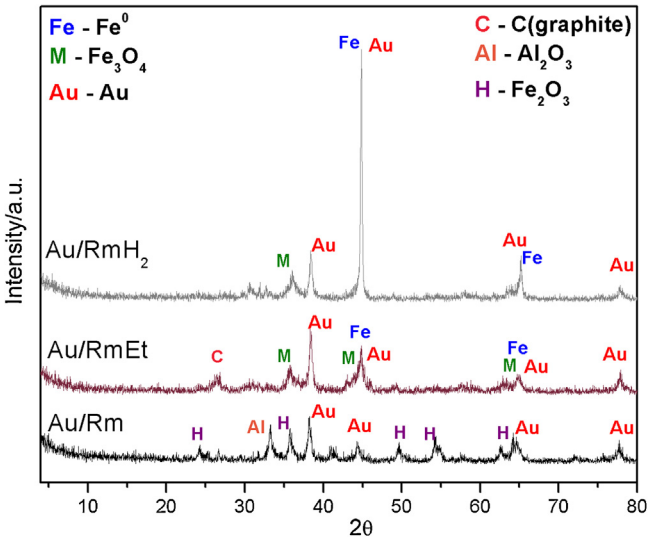

Fig. 1. XRD patterns obtained for samples Au/Rm, Au/RmH_2 and Au/RmEt.

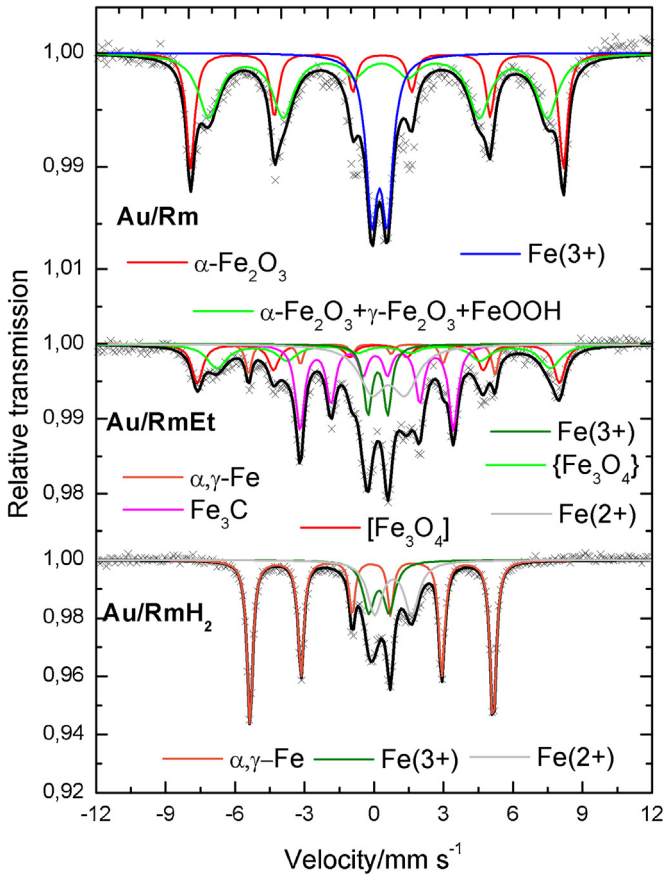

Fig. 2. Room temperature Mössbauer spectra obtained for the prepared catalysts based on red mud.

elements of Rm have not been identified due to overlapping or even to good dispersion of these phases. The catalyst Au/RmEt has no peaks related to hematite, but to magnetite (PDF 1-1111) and metallic iron (PDF 1-1267). One peak associated with the diffraction of graphitic carbon is also identified near 2θ 26° (PDF 26-1077), as a consequence of CVD process with carbon deposition. The XRD pattern obtained for sample Au/RmH$_2$ presents two well defined and intense peaks associated with the formation of Fe^0, which were expected due to prior reduction of Rm during synthesis of the support. A less intense peak can also be seen with 2θ angle equals to 36, correspondent to magnetite phase.

In order to better characterize the iron phases formed in the catalysts prepared with Au and Rm and confirm the results of XRD and TPR, the materials were analyzed by Mössbauer spectroscopy. Fig. 2 shows the spectra obtained for the gold catalysts based on Rm.

In Table 1 the hyperfine parameters used to determine the iron phases present in the samples analyzed by Mössbauer spectroscopy are organized. Furthermore, in Table 1 it is also possible to obtain information concerning the relative percentage of each phase in the samples.

By Mössbauer spectroscopy it is possible to confirm the presence of hematite in the red mud, represented by a sextet defined with hyperfine parameters characteristic of the phase α-Fe$_2$O$_3$ (26% of relative spectral area), and a phase of superparamagnetic iron III (28%) represented by a well-defined doublet in the central region of the spectrum (Fig. 2, Table 1). The other phase identified in the sample Au/Rm is a transition phase consisting of a mix of hematite, maghemite and goethite, α-Fe$_2$O$_3$, γ-Fe$_2$O$_3$ and FeOOH (46% relative area for the three phases), all containing Fe^{3+}. In the catalyst prepared with reduced red mud, Au/RmH$_2$, there are no signals

Table 1
Mössbauer hyperfine parameters used in the determination of iron phases present in the catalysts produced with Red mud.

Sample	Site/Phase	δ/mm s^{-1} (0.05)	ΔQ/mm s^{-1} (0.05)	B_{hf}/T (0.05)	Area/%
Au/Rm	α-Fe$_2$O$_3$	0.34	−0.23	49.8	26
	α-Fe$_2$O$_3$ + γ-Fe$_2$O$_3$ + FeOOH	0.34	−0.13	45.3	46
	Fe(3+)	0.34	0.67	–	28
Au/RmEt	α,γ-Fe	0.0	0.0	33.0	7
	{Fe$_3$O$_4$}	0.51	0.02	45.0	16
	[Fe$_3$O$_4$]	0.28	−0.03	48.4	18
	Fe$_3$C	0.18	0.00	20.5	28
	Fe(3+)	0.26	0.85	–	10
	Fe(2+)	0.72	1.42	–	21
Au/RmH$_2$	α,γ-Fe	0.0	0.0	33.0	59
	Fe(3+)	0.31	0.89	–	17
	Fe(2+)	0.92	1.59	–	24

δ – isomeric shift on the α-Fe; ε – quadrupole shift; Δ – quadrupole splitting; B$_{hf}$ – hyperfine magnetic field; AR – subspectral relative area; {} – octahedral site; [] – tetrahedral site.

related to α-Fe$_2$O$_3$, γ-Fe$_2$O$_3$ or FeOOH, but signals of Fe^{2+} (24%) and metallic iron (α,γ-Fe) with relative area of 59%. The phase Fe^{3+} superparamagnetic is still present, but with lower relative percentage, 17%. These identified Fe^{3+} and Fe^{2+} phases show hyperfine parameters characteristic of iron silicates [12], what explains why they do not suffer reduction during the synthesis of the catalysts. In the case of the catalyst produced with RmEt, it is possible to identify the species Fe^{3+} (10%), Fe^{2+} (21%) and α,γ-Fe (7%). However, the sample Au/RmEt has magnetite (Fe$_3$O$_4$) in its composition, with octahedral (16% spectral area) and tetrahedral sites (18%), in addition to iron carbide, Fe$_3$C (28%), formed by the reaction of carbon deposited from ethanol and iron species during CVD synthesis of the support. The catalysts produced with gold nanoparticles supported on different supports based on Rm underwent thermal analysis, TG and DTA. The results are shown in Fig. 3.

TG curves presented in Fig. 3(a) show a weight loss of ca. 2% up to 100 °C for all samples, which is associated with loss of hydration water. For the sample Au/Rm, there is a slight weight loss of approximately 4% during the entire experiment that may refer to the decomposition of iron oxy-hydroxide specie (goethite – FeOOH), which is unstable at high temperatures. The goethite decomposition produces hematite due to loss of water, according to the following equation:

$$\mathrm{FeOOH} \rightarrow \mathrm{Fe_2O_3} + \mathrm{H_2O} \quad (1)$$

The TG curve obtained for the sample Au/RmH$_2$ presents a significant weight gain of about 10%, which starts after 200 °C and is associated with oxidation of Fe reduced phases. This result is consistent with previous results of XRD and Mössbauer that showed high concentration of Fe^0 in Au/RmH$_2$ composition.

The catalyst Au/RmEt presents a TG curve with two important events: (i) weight gain of 8% starting at 240 °C and (ii) weight loss of 25% from 380 °C up 680 °C. The first event is associated with oxidation of reduced iron phases. According to results of XRD and Mössbauer spectroscopy, the catalyst Au/RmEt has magnetite and metallic iron in its composition, which are oxidized by oxygen to hematite from 240 °C on. The event of weight loss is related to carbon oxidation that produces gaseous species, such as CO and CO$_2$. This weight loss is directly related to the carbon content of the material, which was also determined by elemental analysis that confirmed the content of approximately 25% C.

The DTA curves (Fig. 3(b)) obtained for samples Au/RmH$_2$ and Au/RmEt show two peaks partially overlapped by approximately 290 and 360 °C that are associated to the exothermic oxidation of Fe^0 to Fe^{2+} and Fe^{2+} to Fe^{3+}, respectively. The DTA curve of the

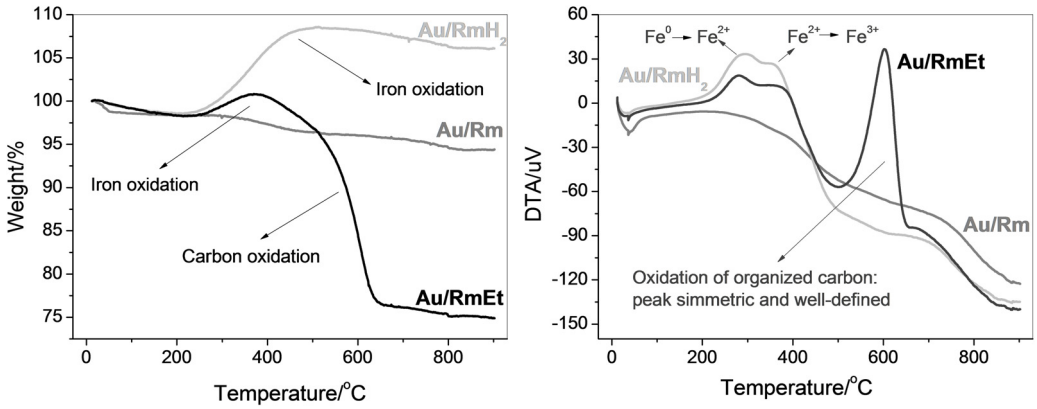

Fig. 3. (a) TG and (b) DTA curves obtained under air atmosphere for the catalysts.

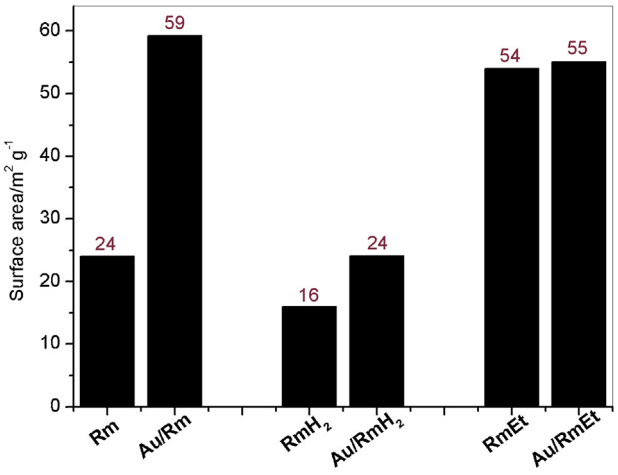

Fig. 4. BET specific surface area values for the catalysts and their respective supports.

sample Au/Rm shows no peaks in this region, since the Rm support has only Fe^{3+} phases, as evidenced by prior techniques. In addition to the peaks relating to iron oxidation, the DTA curve of Au/RmEt still shows a very strong and well-defined peak centered on 600 °C and corresponding to exothermic carbon oxidation. The symmetrical shape of this peak suggests that the carbon presented on the support RmEt is in the form of organized and homogeneous carbon structures, such as nanotubes, nanofibers or graphitic carbon, even after impregnation with gold nanoparticles.

Measurements of the surface area and porosity were made by N_2 adsorption/desorption by the BET method for both the supports and the catalysts prepared with Au nanoparticles. Fig. 4 shows a comparison between the surface area values obtained for the gold catalysts and their supports.

In Fig. 4 it can be seen that, in general, impregnation of Au on the support increases its surface area. This increase is more significant for the catalyst prepared with pure Rm, since this waste comprises an agglomerate of large particles and few pores with low surface area, as observed in SEM images. After reduction of Rm with H_2 at 700 °C for 3 h, the support RmH_2 is produced, with even smaller surface area, mainly due to sintering effects arising from the temperature. It is described in literature that the presence of sodium and calcium oxides is responsible for Rm sintering at high temperatures [16]. The support RmEt already has a surface area higher than other materials because of the carbon structures deposited during CVD process. As it can be seen in the SEM image of Fig. 5, the carbon filaments formed contribute greatly to the increase of surface area. In this case, the impregnation with gold did not increase significantly the surface area, suggesting that this property is mainly influenced by the carbon coating.

The prepared catalysts were analyzed by scanning electron microscopy (SEM). In Fig. 5 images obtained for pure supports (Rm, RmH_2 and RmEt) and for the catalysts prepared by impregnation of Au nanoparticles on the support surfaces can be observed.

It is observed in SEM images of Fig. 5 that the supports maintain their morphological characteristics after impregnation with Au. Rm and RmH_2 present a typical irregular morphology of oxides. RmEt presents several filaments all over the matrix. After Au impregnation all supports present small bright spots inherent to the metallic gold nanoparticles well dispersed on the supports. This is because SEM images of the catalysts were obtained by backscattered electrons, which generate contrast between regions of different compositions. Therefore, it is possible to say that gold was deposited on the surface of materials in the form of nanoparticles with approximate dimensions between 40 and 70 nm.

Additionally, the catalysts as well as the pure supports were analyzed by EDS microanalysis. Fig. 6 shows EDS spectra corresponding to samples RmH_2 and Au/RmH_2.

The first EDS spectrum of Fig. 6 shows that the support RmH_2 has the elemental composition typical of Rm: Fe, Si, Na, Ca, Ti, Al, K and P, usually in the form of oxides [33]. EDS spectrum generated by the sample of the catalyst prepared with Au supported in RmH_2 shows the same peaks of the first spectrum beside peaks characteristic of gold. It is important to note that EDS analysis is qualitative and cannot provide information about the relative amount of elements present in both samples.

TEM images were obtained in order to better characterize the gold nanoparticles supported on different red mud based supports (Fig. 7). The presence of carbon filaments in the composite Au/RmEt is remarkable, especially as multiwalled carbon nanotubes. The Au nanoparticles decorate those filaments, being well dispersed all over the carbon nanostructures. Some Fe nanoparticles encapsulated by carbon can also be identified in TEM images of Au/RmEt. TEM images obtained of the catalyst Au/RmH_2 show gold nanoparticles very well dispersed on the surface of reduced red mud.

Based on TEM images, the size distribution of Au particles was carried out for each of the catalysts produced and the distribution graphs can be seen in Fig. 8. The distribution was carried out using *ImageJ* software. It is observed in that both the distribution and the average size of Au nanoparticles deposited on the catalysts Au/Rm and Au/RmEt are very similar, 28 and 30 nm respectively. However, the catalyst Au/RmH_2 presents larger particles and has a wider distribution suggesting that the impregnation was not very homogeneous. Since the method used for impregnation of Au nanoparticles was the same for all three catalysts produced, this difference is probably related to characteristics of the support. The

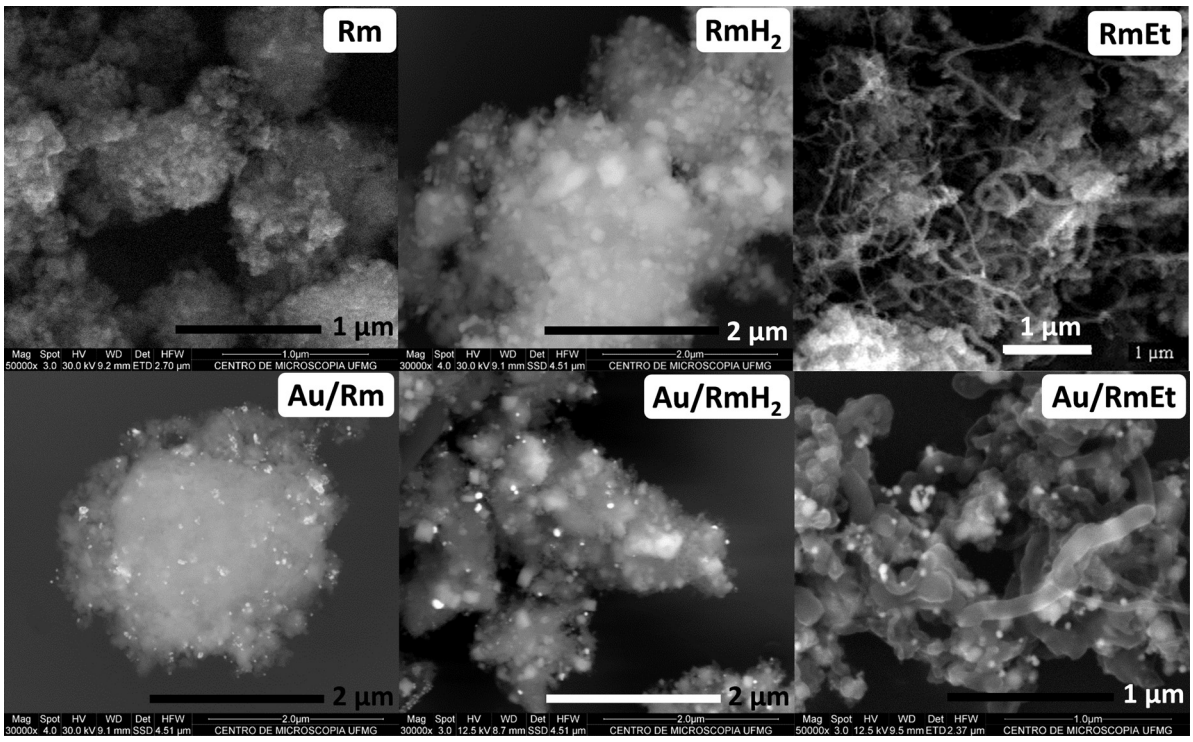

Fig. 5. SEM images obtained for the supports Rm, RmH_2 and RmEt and the catalysts prepared with gold.

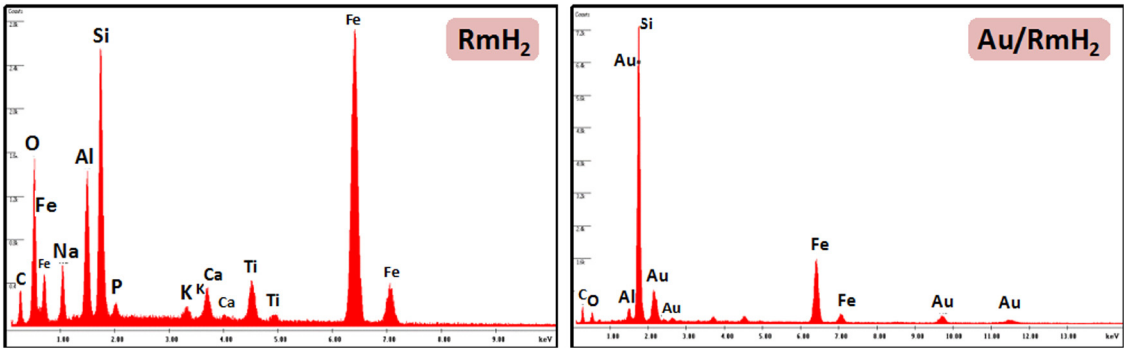

Fig. 6. EDS spectra corresponding to samples RmH_2 and Au/RmH_2.

support RmH_2 is less porous, with the surface area smaller than the proper starting material, the red mud, as it was shown by the BET method. As this material is more compact with very low specific surface area the dispersion of small Au particles is not favored.

Leaching tests in aqueous solution were carried out by atomic absorption spectrometry and showed no significant leaching of Au, less than 1% of the total content for all catalysts produced.

3.1. Catalytic reactions

All samples were tested for dibenzothiophene (DBT) oxidation with H_2O_2 in biphasic system. The biphasic system is necessary since DBT is an organic liposoluble molecule and the oxidant H_2O_2 is very hydrosoluble. DBT removal from organic phase was monitored by UV–vis after 120 min of reaction. The graph in Fig. 9 shows DBT oxidation results in terms of the content of S oxidized by the amount of catalyst used (mg $S/g_{catalyst}$).

It is observed in Fig. 9 that gold nanoparticles supported on pure red mud and reduced red mud do not increase the efficiency of these supports on the DBT oxidation. On the other hand, the catalyst Au/RmEt exhibits a remarkable capacity to catalyze DBT oxidation in comparison with the other catalysts prepared. Au/RmEt is twice more efficient than Au/RmH_2 and Au/Rm. The pure support RmEt also stands as a good catalyst when compared to the other pure supports.

It is proposed that DBT oxidation occurs via the Fenton mechanism, where H_2O_2 is activated by iron species to form $HO^{\bullet}$ radicals. This process is very well discussed in the literature [21,23,34–38].

Catalysts reactivity towards the Fenton chemistry can be discussed in terms of their composition of iron species. The presence of Fe^{2+} species on the catalyst surface is essential for a high activity towards H_2O_2 reaction, since it is well known from the literature that $Fe^{2+}{}_{surf}$ can initiate the reaction by the generation of $HO^{\bullet}$ radicals via a Haber–Weiss mechanism (Equation (2)):

$$Fe^{2+}{}_{surf.} + H_2O_2 \rightarrow {}^{\bullet}OH + OH^{-} + Fe^{3+}{}_{surf.} \quad (2)$$

Comparing the different red mud supports, i.e. Rm, RmH_2 and RmEt, we can observe that pure Rm contains only Fe^{3+} oxides, hematite (α-Fe_2O_3) and maghemite (γ-Fe_2O_3), which are nearly inactive for H_2O_2 decomposition. We also observe that pure Rm leachates iron species into aqueous phase. These iron species dispersed in water are likely active for homogeneous Fenton [39]. The

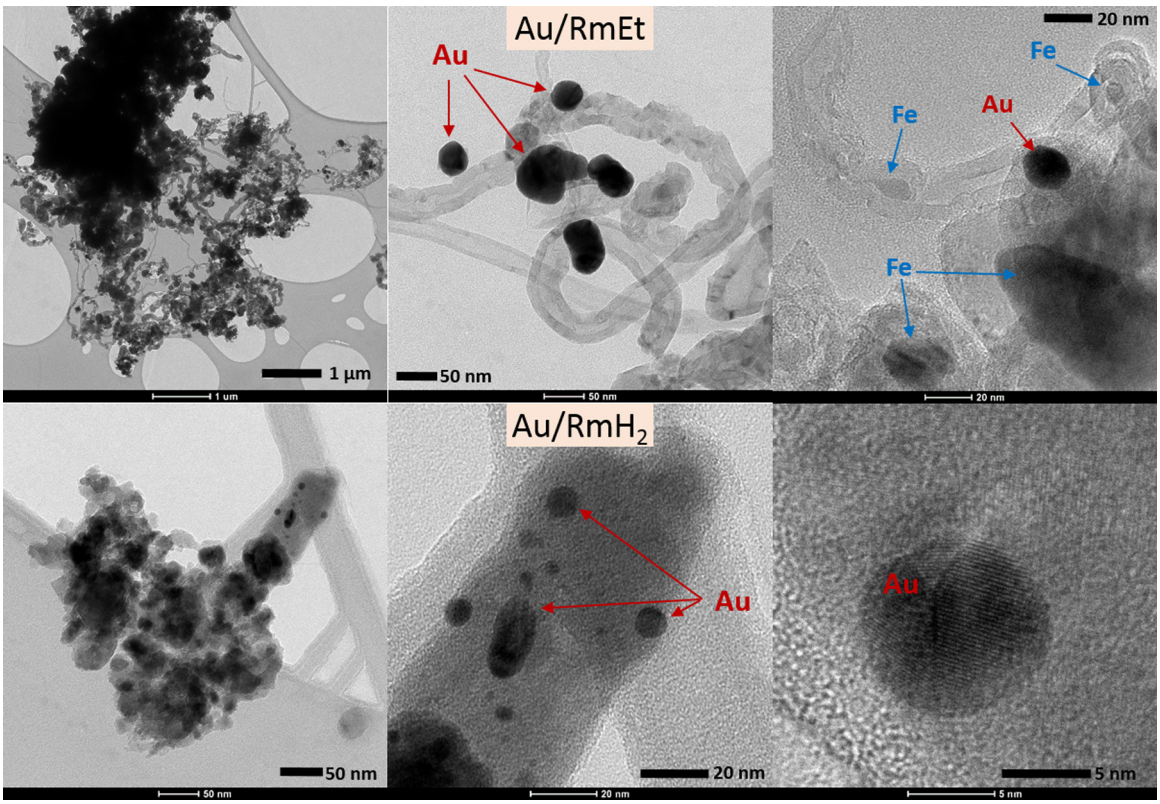

Fig. 7. TEM images obtained for catalysts Au/RmEt and Au/RmH_2.

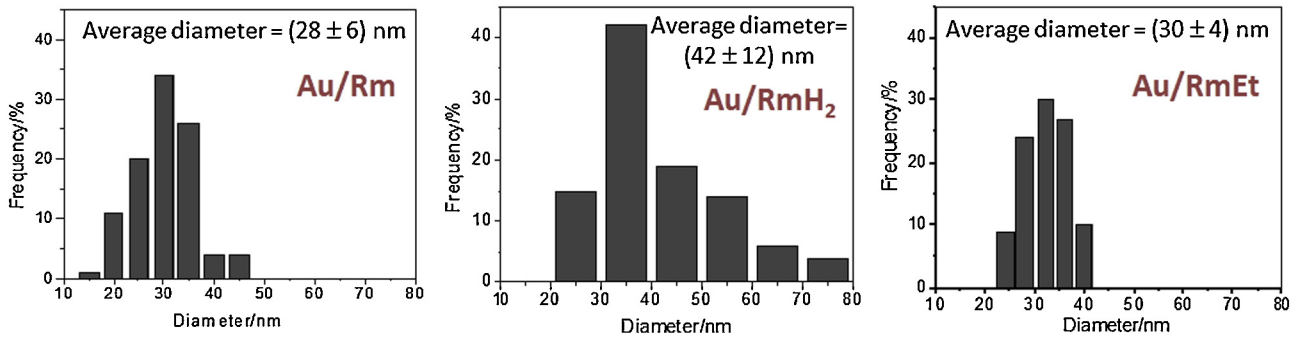

Fig. 8. Particle size distribution of Au on the catalysts Au/Rm, Au/RmH_2 and Au/RmEt.

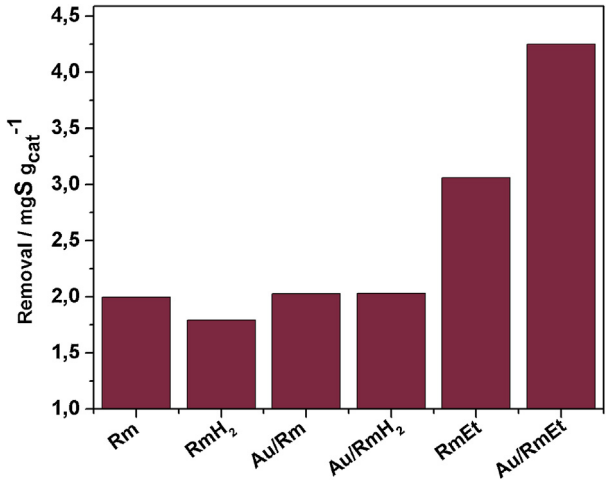

Fig. 9. Removal of dibenzothiophene after 120 min of reaction (5 mL DBT 50 ppm S in cyclohexane, 1 mL H_2O_2(aq) 30% and 20 mg catalysts).

reduction of red mud with hydrogen (in RmH_2) produced metallic iron, Fe^0, a potential three electrons donor. Metallic iron has been studied as chemical reducer for different organic contaminants in water. However, the direct electron transfer from Fe^0 to H_2O_2 in a Haber–Weiss like mechanism is a very slow process in a near neutral pH medium. For these reasons, samples Rm and RmH_2 show very low activity for DBT oxidation. The high activity presented by RmEt can also be associated with its iron composition. During the CVD process of Rm with ethanol, 34% of magnetite (Fe_3O_4) and 7% of metallic iron (Fe^0) are produced. Fe_3O_4 is an oxide that contains Fe^{2+}, which means that it is able to activate hydrogen peroxide. In addition, the combination of Fe^0 with Fe_3O_4 can improve the electron transfer from Fe_3O_4 to H_2O_2 to form $^{\bullet}OH$ radicals by Haber–Weiss reaction. The combination of Fe^0 and Fe_3O_4 create an interface metal–oxide and the possibility of electron transfer from Fe^0 to the oxide. The interface metal–semiconductor is known to form an Ohmic junction with very low resistance [34,36].

Catalysts Au/Rm, Au/RmH_2 and Au/RmEt present different behaviors in biphasic systems, as shown by images of Fig. 10.

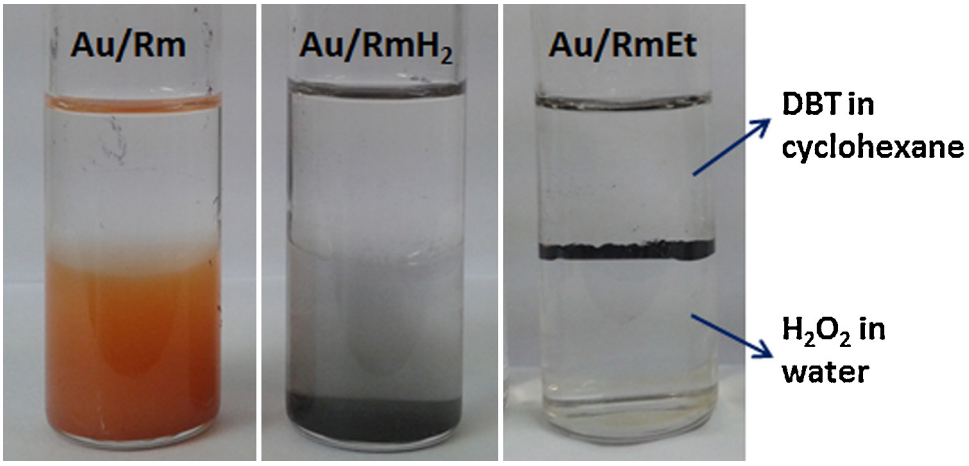

Fig. 10. Images of gold catalysts in biphasic systems.

It is clearly seen in Fig. 10 that catalysts prepared with pure Rm and reduced Rm (RmH_2) disperse only into the aqueous phase, mainly due to their high hydrophilic character. Thus, their catalytic properties are limited by the interface, since the DBT substrate is in the organic phase. Moreover, the pure residue is partially soluble in aqueous phase and leaches undesired metals to the system that cannot be removed magnetically. On the other hand, the catalyst produced with RmEt (prepared via CVD of Rm and ethanol) locates preferentially at the interface of immiscible phases, which means that it is an amphiphilic catalyst. Au/RmEt may interact at the same time with the aqueous phase containing the oxidant and the organic phase containing the S contaminant.

It is known that gold nanoparticles have a great affinity to sulfur, since Au-S form a pair of soft acid–base [32]. However, in the absence of the active iron phase (Fe^{2+}), *i.e.* in Au/Rm or Au/RmH_2 catalysts, Au shows no activity in the oxidation process *via* the Fenton mechanism. On the other hand, in Au/RmEt, a synergistic effect between supported Au nanoparticles and Fe^{2+} nuclei from red mud is observed. The amphiphilic support itself, RmEt, presents good efficiency in DBT removal due to its $Fe^{2+}{}_{surf}$ and to its amphiphilic property, as discussed previously. Additionally, the presence of Au in the catalyst Au/RmEt contributes to the activity of the support, much more than in Au/Rm and Au/RmH_2. In the synergistic effect gold acts as a facilitator of the reaction by adsorbing DBT molecules [32] prior to the oxidation by $^{\bullet}OH$ radicals formed by $Fe^{2+}{}_{surf}$ cores of RmEt. Fig. 11 shows a schematic mechanism of the synergistic effect between Au and Fe in the catalyst Au/RmEt.

The first frame of Fig. 11 shows the catalyst in contact with organic and aqueous phases in a biphasic system. The catalyst is represented as a hydrophilic matrix composed of thermally stable oxides of red mud, such as SiO_2 and Al_2O_3. On the surface of the matrix are cores of Fe^0 and Fe_3O_4, which are responsible for the Fenton-like reaction (formation of hydroxyl radicals). A partial carbon coating of the matrix is also represented. The carbon nanofilaments are responsible for the hydrophobic portion of the catalyst, which enables its interaction also with organic phases.

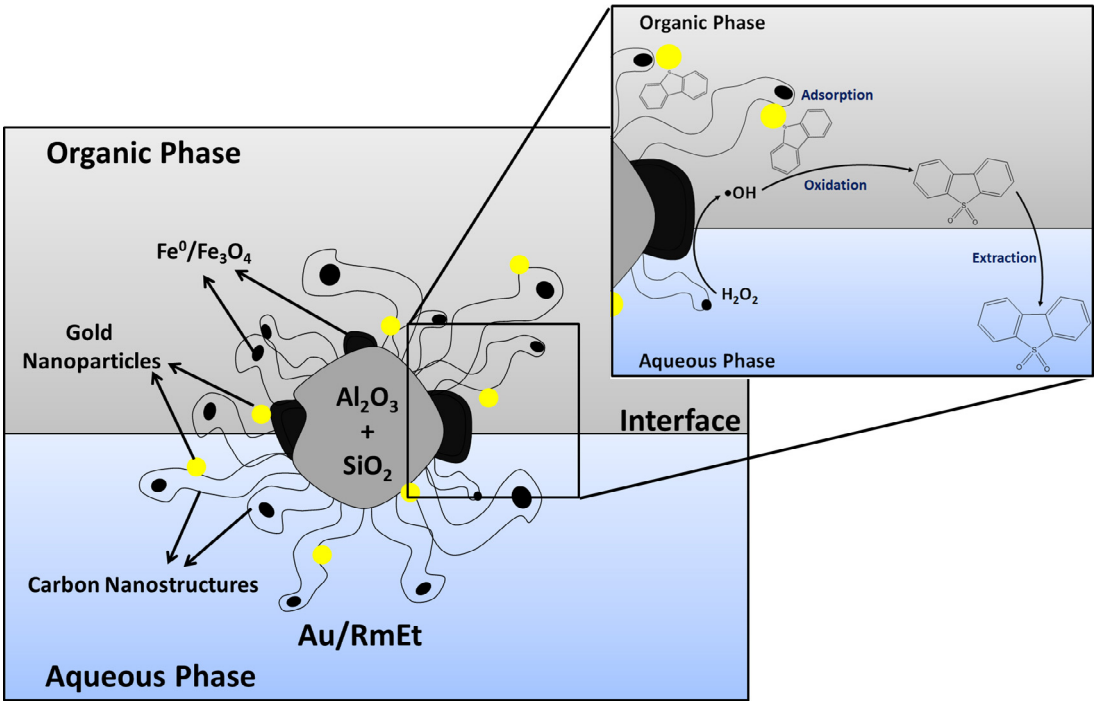

Fig. 11. Mechanism of synergistic effect between Au and Fe.

Moreover, Au nanoparticles are supported on the top of this complex structure. In the second frame of the schematic mechanism the synergistic effect is shown in detail. Gold nanoparticles adsorb DBT molecules due to an interaction between Au and S (soft acid–base pair). Right close, $^{\bullet}OH$ radicals are formed and quickly oxidize the DBT molecules adsorbed.

4. Conclusions

Catalysts were prepared in this work with gold nanoparticles supported on different matrixes based on red mud waste: (i) pure red mud – Au/Rm, (ii) reduced red mud – Au/RmH$_2$ and (iii) partially carbon coated red mud – Au/RmEt. Results showed that gold nanoparticles were very well dispersed on the surface of supports with average diameter of 30 nm. The catalysts were applied in biphasic desulfurization reactions with H_2O_2 and the catalyst Au/RmEt showed a remarkable efficiency in comparison with the other red mud based catalysts. While Au/Rm and Au/RmH$_2$ are hydrophilic and stay in the aqueous phase, Au/RmEt presents high affinity for both organic and aqueous phase locating at the interface of the biphasic system, which enables a synergistic effect between gold and iron phases of red mud. Gold nanoparticles adsorb sulfur contaminants and simultaneously Fe^{2+}_{surf} sites activate H_2O_2, promoting DBT oxidation.

Acknowledgments

The authors would like to acknowledge PETROBRAS, CNPq, CAPES, FAPEMIG for financial support and also the Center of Microscopy at the Universidade Federal de Minas Gerais (http://www.microscopia.ufmg.br) for providing the equipment and technical support for experiments involving electron microscopy.

Appendix A. Supplementary data

Supplementary data associated with this article can be found, in the online version, at http://dx.doi.org/10.1016/j.apcatb.2014.07.003.

References

[1] S. Kumar, R. Kumar, A. Bandopadhyay, Resour. Conserv. Recycl. 48 (2006) 301–314.
[2] J. Rivas Mercury, A.A. Cabral, A.E.M. Paiva, R.S. Angelica, R.F. Neves, T. Scheller, J. Therm. Anal. Calorim. 104 (2011) 635–643.
[3] A. Gelencsér, N. Kováts, B. Turóczi, Á. Rostási, A. Hoffer, K. Imre, I. Nyirő-Kósa, D. Csákberényi-Malasics, Á. Tóth, A. Czitrovszky, A. Nagy, S. Nagy, A. Ács, A. Kovács, Á. Ferincz, Z. Hartyáni, M. Pósfai, Environ. Sci. Technol. 45 (2011) 1608–1615.
[4] S.B. Wang, H.M. Ang, M.O. Tade, Chemosphere 72 (2008) 1621–1635.
[5] S. Sushil, V.S. Batra, Appl. Catal. B: Environ. 81 (2008) 64–77.
[6] N.A. Hodge, C.J. Kiely, R. Whyman, M.R.H. Siddiqui, G.J. Hutchings, Q.A. Pankhurst, F.E. Wagner, R.R. Rajaram, S.E. Golunski, Catal. Today 72 (2002) 133–144.
[7] K.C. Pratt, V. Christoverson, Fuel 61 (1982) 460–462.
[8] A. Eamsiri, W.R. Jackson, K.C. Pratt, V. Christov, M. Marshall, Fuel 71 (1992) 449–453.
[9] A.M. Mastral, C. Mayoral, M.T. Izquierdo, C. Pardos, Fuel Process. Technol. 36 (1993) 177–184.
[10] S. Yokoyama, M. Yamamoto, Y. Maekawa, T. Kotanigawa, Fuel 68 (1989) 531–533.
[11] B. Klopries, W. Hodek, F. Bandermann, Fuel 69 (1990) 448–455.
[12] E. Karimi, I.F. Teixeira, L.P. Ribeiro, A. Gomez, R.M. Lago, G. Penner, S.W. Kycia, M. Schlaf, Catal. Today 190 (2012) 73–88.
[13] E. Karimi, I.F. Teixeira, A. Gomez, E. de Resende, C. Gissane, J. Leitch, V. Jollet, I. Aigner, F. Berruti, C. Briens, P. Fransham, B. Hoff, N. Schrier, R.M. Lago, S.W. Kycia, R. Heck, M. Schlaf, Appl. Catal. B: Environ. 145 (2014) 187–196.
[14] B.K. Yathavan, F.A. Agblevor, Energy Fuels 27 (2013) 6858–6865.
[15] A.I. Cakici, J. Yanik, S.U. Çar, T. Karayildirim, H. Anil, J. Mater. Cycles Waste Manag. 6 (2004) 20–26.
[16] J.R. Paredes, S. Ordonez, A. Vega, F.V. Diez, Appl. Catal. B: Environ. 47 (2004) 37–45.
[17] P.F. Ng, L. Li, S.B. Wang, Z.H. Zhu, G.Q. Lu, Z.F. Yan, Environ. Sci. Technol. 41 (2007) 3758–3762.
[18] I.F. Teixeira, T.P.V. Medeiros, P.E. Freitas, M.G. Rosmaninho, J.D. Ardisson, R.M. Lago, Fuel 124 (2014) 7–13.
[19] S.E. Khalafalla, L.A. Haas, J. Catal. 24 (1972) 115–120.
[20] Q. Liu, R. Xin, C. Li, C. Xu, J. Yang, J. Environ. Sci. 25 (2013) 823–829.
[21] A.A.S. Oliveira, I.F. Teixeira, T. Christofani, J.C. Tristão, I.R. Guimarães, F.C.C. Moura, Appl. Catal. B: Environ. 144 (2014) 144–151.
[22] A.A.S. Oliveira, I.F. Teixeira, L.P. Ribeiro, J.C. Tristao, A. Dias, R.M. Lago, J. Braz. Chem. Soc. 21 (2010) 2184–2188.
[23] R.C.C. Costa, F.C.C. Moura, P.E.F. Oliveira, F. Magalhães, J.D. Ardisson, R.M. Lago, Chemosphere 78 (2010) 1116–1120.
[24] S. Muhammad, E. Saputra, H. Sun, H.-M. Ang, M.O. Tadé, S. Wang, Ind. Eng. Chem. Res. 51 (2012) 15351–15359.
[25] A.A.S. Oliveira, I.F. Teixeira, L.P. Ribeiro, E. Lorençon, J.D. Ardisson, L. Fernandez-Outon, W.A.A. Macedo, F.C.C. Moura, Appl. Catal. A: Gen. 456 (2013) 126–134.
[26] I.F. Teixeira, A.A.D.S. Oliveira, T. Christofani, F.C.C. Moura, J. Mater. Chem. A 1 (2013) 10203–10208.
[27] W.F. de Souza, I.R. Guimaraes, M.C. Guerreiro, L.C.A. Oliveira, Appl. Catal. A: Gen. 360 (2009) 205–209.
[28] W.F. Souza, I.R. Guimarães, D.Q. Lima, C.L.T. Silva, L.C.A. Oliveira, Energy Fuels 23 (2009) 4426–4430.
[29] C. Song, Catal. Today 86 (2003) 211–263.
[30] L. Pasquali, F. Terzi, M. Montecchi, B.P. Doyle, J. Lukkari, B. Zanfrognini, R. Seeber, S. Nannarone, J. Electron Spectrosc. Relat. Phenom. 172 (2009) 114–119.
[31] J. Noh, S. Jang, D. Lee, S. Shin, Y.J. Ko, E. Ito, S.-W. Joo, Curr. Appl. Phys. 7 (2007) 605–610.
[32] J.A. Rodriguez, P. Liu, Y. Takahashi, K. Nakamura, F. Vin˜es, F. Illas, J. Am. Chem. Soc. 131 (2009) 8595–8602.
[33] E. Saputra, S. Muhammad, H. Sun, H.M. Ang, M.O. Tadé, S. Wang, Catal. Today 190 (2012) 68–72.
[34] F.C.C. Moura, M.H. Araujo, R.C.C. Costa, J.D. Fabris, J.D. Ardisson, W.A.A. Macedo, R.M. Lago, Chemosphere 60 (2005) 1118–1123.
[35] R.F.B. Nogueira, A.G. Trovó, M.R.A. Silva, R.D. Villa, Quim Nova 30 (2007) 400–408.
[36] R.C.C. Costa, F.C.C. Moura, J.D. Ardisson, J.D. Fabris, R.M. Lago, Appl. Catal. B: Environ. 83 (2008) 131–139.
[37] A.C. Aguiar, D. Rodríguez, J. Quim. Nova 30 (2007) 623–628.
[38] I.S.X. Pinto, P.H.V.V. Pacheco, J.V. Coelho, E. Lorençon, J.D. Ardisson, J.D. Fabris, P.P. de Souza, K.W.H. Krambrock, L.C.A. Oliveira, M.C. Pereira, Appl. Catal. B: Environ. 119–120 (2012) 175–182.
[39] F.C.C. Moura, G.C. Oliveira, M.H. Araujo, J.D. Ardisson, W.A.D.A. Macedo, R.M. Lago, Chem. Lett. 34 (2005) 1172–1173.